DEVELOPMENT OF A SEMI-DISTRIBUTED INTERFEROMETER FOR SALIVA-BASED DETECTION OF IL-6 AND IL-8 IN ORAL SQUAMOUS CELL CARINOMA

Aida Zhakypbekova, Bachelor of Biological Sciences

Submitted in fulfillment of the requirements for the degree of a Master of Science in Biomedical Engineering

School of Engineering and Digital Sciences
Department of Chemical and Materials Engineering
Nazarbayev University

53 Kabanbay Batyr Avenue,
Nur-Sultan, Kazakhstan, 010000

Supervisors:

Lead Supervisor Name: Professor Daniele Tosi

Co-supervisor Name: Associate Professor Cevat Erisken

April 2025

Declaration

I hereby declare that this manuscript, entitled “Development of a Semi-Distributed Interferometer for Saliva-Based Detection of IL-6 and IL-8 in Oral Squamous Cell Carcinoma” is the result of my work except for quotations and citations which have been duly acknowledged.

I also declare that, to the best of my knowledge and belief, it has not been previously or concurrently submitted, in whole or in part, for any other degree or diploma at Nazarbayev University or any other national or international institution.

Name Aida Zhakypbekova

Date: 04.04.2025

Acknowledgements

I wish to acknowledge the invaluable contributions of all the individuals who helped me throughout this journey. First and foremost, I would like to express my deepest gratitude to my supervisor, Professor Daniele Tosi, for his continuous guidance, patience and support. His expertise and mentorship, especially during data analysis, helped me grow both academically and personally.

I am also thankful to the members of the Laboratory of Biosensors and Bioinstruments for their support and assistance with the experiments. In particular, I would like to mention Aliya Bekmurzayeva, Senior Researcher, for her experience and comments, Marzhan Nurlanova, Sabira Seipetdenova, and Kuanysh Seitkamal for their advice and assistance in the lab.

I extend my heartfelt thanks to my family for their endless love and belief in me. This thesis would not have been possible without their unwavering support.

Table of Contents

List of Abbreviations

OSCC	Oral squamous cell carcinoma
IL	Interleukin
SDI	Semi-distributed interferometer
FBG	Fiber Bragg grating
PBS	Phosphate-buffered saline
LoD	Limit of detection
ELISA	Enzyme-Linked Immunosorbent Assay
TNF	Tumor necrosis factor
JAK/STAT	Janus kinase/signal transducer and activator of transcription
MAPK	Mitogen-activated protein kinase
PI3K	Phosphatidylinositol 3-kinase
SERS	Surface-enhanced Raman spectroscopy
EIS	Electrochemical impedance spectroscopy
PDF	Probability density function
RI	Refractive index
RIU	Refractive index units
EBF	Enhanced backscattering fiber
GA	Glutaraldehyde
SMF	Standard single-mode fibers
APTMS	(3-Aminopryl)trimethoxysilane
m-PEG	methoxypolyethylene glycol

List of figures and tables

Abstract

Biomarker-based diagnostics offer a promising approach for early cancer detection, while simultaneous analysis of multiple biomarkers can further improve disease diagnosis by enhancing sensitivity and specificity of the detection. Although blood-based tests are widely used for the analysis of biomarkers, they have several limitations such as invasive sampling, the requirement of trained personnel, and specialized laboratory equipment. Saliva, on the other hand, as an easily accessible and non-invasive biofluid, has gained great attention as a diagnostic fluid. Due to its close association with the oral cavity saliva has been extensively investigated as a means of diagnosing oral squamous cell carcinoma (OSCC). Among diagnostic biomolecules, concentrations of interleukin-6 (IL-6) and interleukin (IL-8) are highly correlated with OSCC development. Therefore, in this work, functionalized fiber-optic biosensor based on semi-distributed interferometer (SDI) was developed for joint detection of IL-6 and IL-8 biomarkers in saliva.

The biosensor is fabricated in a simple and fast way with <1 minute fabrication time and entirely based on a common arc-fusion splicer. Surface of the biosensor is then biofunctionalized to attach antibodies specific to the biomarkers of choice. The detection system is telecom-fiber oriented and occurs real-time at room temperature using a commercially available multi-channel Fiber-Bragg grating (FBG) analyzer. As a proof-of-concept study, the detection was first validated in phosphate buffered saline (PBS) and then in artificial saliva doped with biomarkers.

The data analysis strategy is based on a multi-resonance approach and takes advantage of the entire spectral features, which enhances the robustness and reliability of the detection results. Unlike single-feature approaches, multi-resonance analysis ensures greater resilience to spectral distortions, since the spectral features of the proposed sensor exhibit varying sensitivity to biomolecular interactions. This analysis showed that the sensor demonstrated a limit of detection (LoD) of 480 aM for IL-6 and 23.4 fM for IL-8 in artificial saliva with high specificity to target proteins. It successfully confirmed the ability to distinguish non-target proteins (CD44 and TNF-α).

Keywords: Optical biosensor, multi-resonance analysis, IL-6, IL-8, OSCC, point-of-care diagnostics, semi-distributed interferometer, biomarker detection, surface functionalization

Chapter 1 – (Introduction)

1.1 Saliva as a diagnostic biofluid

1.1.1 Saliva and its composition

Saliva is a body fluid secreted by major and minor salivary glands to protect oral cavity, lubricate and start digestion of food. Major salivary glands include pairs of parotid, submandibular, and sublingual glands. 90% secreted saliva is from major salivary glands, whereas minor salivary glands also found throughout oral cavity are responsible for the rest [1]. On average approximately 0.5 to 1.5 liters of saliva is produced daily [2]. It mainly consists of water (99%), electrolytes, digestive enzymes and various metabolites [2]. Salivary glands are enveloped by capillaries and are highly permeable to biomolecules present in blood [3]. Therefore, it can closely mirror the composition of blood. Depending on the type of analyte passive diffusion, ultrafiltration, and active transport are mechanisms through which biomolecules are transferred to saliva [4]. This feature makes saliva a promising diagnostic biofluid for non-invasive tests.

More than 2000 proteins have been found in saliva, of which approximately 25-30% overlap with those found in blood [5]; the quality of DNA content in saliva, despite the fact that it also contains microbial DNA, is comparable to the DNA in blood [2]; and changes in the concentration of metabolites in blood are consistent with their concentration in saliva [2]. It is essential to recognize that not all components present in blood are transported to saliva, and the suitability of saliva for diagnostic purposes depends on the disease's pathophysiology. The concentration of analytes is often found to be 100-1000 times lower than in blood [6]. In addition, saliva contains macromolecule proteins and mucins that regulate the interaction with various oral microorganisms, by-products of microorganism activity, and endogenous biomolecules produced by salivary glands, epithelial cells, and immune responses in the oral cavity [7]. Therefore, it is important to develop platforms that are exceptionally sensitive and specific for accurate detection of analytes.

1.1.2 Collection of saliva for diagnostic purposes

The process of collecting saliva samples is painless, non-invasive and doesn’t require special equipment or trained personnel, which makes it ideal for children and elderly patients. Main methods of saliva collection are as follows:

The drooling method (Figure 1(a)) is a procedure when patients are asked to open their mouth and tilt their head for saliva to drain from the oral cavity to some collecting containers[8]. The duration of the collection varies from person to person, since the speed of the saliva secretion is different, and the volume for diagnosis varies from technique. The patient's position is called "Coachman's position" [9]. Usually, this procedure is typically performed in children aged three and older to ensure that the patient will remain seated as long as needed. When large amounts of saliva are needed, some sort of stimulation such as applying citric acid is performed before collecting saliva [10].

The spitting method (Figure 1(b)) is more commonly preferred than the drooling method due to its high reproducibility [9]. Patients are asked to gently expel their saliva to some sterile container until the needed volume is achieved [9]. The spitting method is also not very effective for children younger than 3 years which are often uncooperative.

The absorption method (Figure 1(c)) is the most suitable for children [9]. It involves placing some absorbing material, usually cotton swabs, in the oral cavity [9]. This method is utilized in cases where children have difficulties spitting or are uncooperative during the drooling method. It was found that there is no difference regarding the effectiveness of this method between children and adolescents in terms of volume of the saliva obtained and overall applicability.

Lastly, the suction method (Figure 1(d)) requires a special device that aspirates saliva from the patient's oral cavity [10]. Needleless syringes, plastic catheters or pipettes are usually applied to collect saliva in this way. The needed flow rate and volume of saliva can be achieved by stimulating saliva secretion before collection [10]. This method is favored for infants, young children and patients with special conditions [9].

Figure 1. Four methods of saliva collection. (a) the drooling method; (b) the spitting method; (c) the absorption method; (d) the suction method.

1.1.3 Current methods for the quantification of analytes in saliva

Most analytical methods used to detect biomarkers in saliva are limited to laboratory settings due to laborious sample preprocessing, the need for specialized equipment, and trained personnel. In most cases, the enzyme-linked immunosorbent assay (ELISA) is the standard method for the quantification of proteins and peptides [11]. However, ELISA requires multiple washing steps, long incubation times, and can detect only one biomarker at a time, making it inefficient for high-throughput analysis. Its performance is easily influenced by many factors, including solid-phase uniformity, plate washing efficiency, and sample handling conditions. Most importantly, commercially available ELISA kits are not intended to be used on saliva samples. The instructions provided by the manufacturer don’t contain information on how to reduce signals from overlapping molecules that might be present in saliva.

More robust saliva screening is usually performed by liquid chromatography/tandem mass spectrometry, where multiplexed classification of several proteins can be achieved [12]. According to Grocholska et al. [13] over 80% of literature on saliva proteomics and metabolomics is focused on using Liquid Chromatography coupled with Mass Spectrometry and Gas Chromatography coupled with Mass Spectrometry. However, in the case of interleukins, low-abundance salivary proteins, even more advanced techniques such as matrix-assisted laser desorption/ionization time-of-flight are used to ensure high resolution [14]. Most of the literature usually preferred unstimulated saliva to make sure that there are no external influences on the concentration of metabolites and proteins [15].

All these methods require extensive sample preparation steps such protein precipitation, filtration, pH adjustments and stabilization of some intermediate products and so on. Moreover, they rely on expensive equipment and reagents that make the analysis costly, particularly in resource-limited settings. Interfering compounds that absorb light in similar wavelengths or have similar binding groups also lead to inaccurate quantification due to the complex nature of saliva. Most importantly, all these methods require trained personnel, equipment maintenance and data interpretation, which limit its accessibility significantly. Therefore, there is a growing need for new solutions that are simpler, more cost-effective, and accessible to a wider range of users.

1.2 Oral cancer

1.2.1 Oral Squamous Cell Carcinoma: Global Trends and Challenges

Oral squamous cell carcinoma (OSCC) is a subtype of oral cancer, representing over 90% of oral malignancies [16]. In regions where tobacco use, alcohol consumption, and betel quid chewing are prevalent, such as South and Southeast Asia, OSCC accounts for 40% of all cancers [16]. Western countries are commonly associated with Human Papilloma Virus infected cases of OSCC [16]. As with any other type of cancer, early detection is one of the most important aspects of decreasing mortality. According to the National Cancer Institute, the 5-year survival rate for OSCC is 64.4% overall, varying significantly by stage, 83% for early-stage cases and dropping to 38% in advanced stages [17]. Early diagnosis and treatment have also been shown to increase survival rates up to 80% [17]. These challenges highlight the need for improved early detection methods that are accessible to a wide range of populations with high specificity and sensitivity.

OSCC development is a multistep process where premalignant lesions (leukoplakia or erythroplakia) are progressed to invasive carcinoma of epithelium of oral cavities. Although having easy access to visual examinations of the oral cavity, the diagnosis of OSCC is often delayed due to the asymptomatic nature at the beginning and similarities with benign disorders such as oral leukoplakia or erythroplakia [18]. Conventional methods such as palpations and visual inspections are unreliable when it comes to screening cancer. This is driving new diagnosis methods of OSCC in the scientific community.

1.2.2 Current methods of diagnosing oral cancer

There are several visual screening tools that help clinicians in diagnosing OSCC:

Fluorescence imaging. Usually, cancerous tissues appear non-fluorescent when exposed to blue light, while normal oral tissues appear green. Special imaging devices such as VELscope were invented to aid this process of visualization [19].

Toluidine blue staining. This vital dye selectively binds tissues with high proliferative activity, a common characteristic of malignant tissues. This technique guides identification of risk areas for tissue biopsy tests [19].

Brush biopsy. This method offers a less invasive alternative to traditional biopsy, using a soft brush to collect cells from the lesion. These cells are subsequently evaluated under a microscope [19].

Commonly used imaging techniques such as computed tomography, magnetic resonance imaging, positron-emission tomography, and ultrasound are used in later stages to assess the depth and size of the tumor. The sensitivity of these imaging techniques varies between 55 - 80% for MRI and 80% and higher for PET. Therefore, often, they are combined to improve diagnosis accuracy [20].

While gold standard for cancer diagnosis still remains tissue biopsy, a new tool named liquid biopsy is emerging. It utilizes body fluids such as blood, pleural fluid, saliva, and cerebrospinal fluid to detect cancer biomarkers, including circulating tumor cells, circulating tumor DNA, microRNAs, and various proteomic and metabolomic biomolecules. In the context of OSCC, liquid biopsy focuses on analyzing genetic mutations, copy of number variations and methylation patterns in circulating tumor DNA using digital polymerase chain reaction and next-generation sequencing [21].

OSCC has been proven to affect the composition of saliva depending on the stage. Different biomolecules were investigated for the diagnosis of OSCC and to distinguish it from its benign counterparts, including cytokines (IL-8, IL-6, and tumor necrosis factor-α (TNF-α)) [22], salivary enzymes [23], and microRNAs [24]. Among these, abnormal expressions of different cytokines has been widely and consistently reported to link the inflammatory response with the development of OSCC [25]. Their role as key mediators of cell communication enables them to regulate and respond to various cancer-related mechanisms [26]. Studies reported significantly elevated levels of IL-6, IL-8, IL-10, TNF-α, IL-1β, IL-13, IL-4 [25]. However, studies dedicated to the analysis of the combination of IL-6 and IL-8 proteins in the diagnosis of OSCC showed the most promising results. Although cytokine levels can also be affected by other inflammatory conditions such as gingivitis or periodontitis, the extent of these changes

is significantly lower compared to OSCC cases [18]. A large-scale study of gene expression in patients with oral cancer also identified the overexpression of IL-8 and IL-6 unique to OSCC [27]. Another study by John *et al*.[28] proved that the combination of these two cytokines offers a sensitivity of 99% for the diagnosis of OSCC with the specificity remaining high at 90%.

1.3 IL-6 and IL-8 as oral cancer biomarkers

IL-6 is a multifunctional cytokine that is expressed by various cells in the body including macrophages, T-lympocytes, B-lymphocytes, monocytes, fibroblasts and endothelial cells in response to the inflammatory stimuli [26]. It plays a critical role in different physiological and pathological processes, including inflammation, immune responses, and metabolic regulation. The mechanism of action of IL-6 begins with binding to interleukin-6 receptor (IL-6R) which is present in both membrane-bound and soluble forms [29]. This allows IL-6 signaling to expand the inflammatory response and tissue repair capabilities. Upon formation of IL-6 and IL-6R complex, downstream pathways such as Janus kinase/signal transducer and activator of transcription (JAK/STAT) pathway, as well as the mitogen-activated protein kinase (MAPK) and phosphatidylinositol 3-kinase (PI3K) pathways are activated [29]. This signaling network allows IL-6 to contribute to a wide range of biological effects.

IL-8 or CXCL8 is a proinflammatory chemokine, initially known for its chemoattracting properties which assist in migration of neutrophils to the site of inflammation. [26]. It is mainly produced by leukocytes and endothelial cells upon secretion of IL-1 or TNF-α [30]. Alternatively, various stimuli such as hypoxia, reactive oxygen species and different chemotherapeutic agents can also trigger production of IL-8 [30]. There are two receptors CXCR1 (high affinity receptor to IL-8) and CXCR2 (has affinity for various interleukins) through which IL-8 can exert its effects [31]. Both hematopoietic and non-hematopoietic cells express these receptors. Upon binding to receptor, IL-8 activates the MAPK (specifically ERK1/2) and PI3K/AKT pathways, promoting chemotaxis, cell proliferation, and survival [31].

Normal tissues express very low concentrations of these cytokines: levels of IL-8 from 52.1 to 1578 pg/mL, levels of IL-6 varied from 0 to 16 pg/mL in some studies and from 33.4 to 69.2 pg/mL in other studies based on a meta-analysis of 14 articles [32]. According to the same study, in patients with OSCC, their levels were significantly higher, varying from 283.7 and 4082.8 pg/mL for IL-8 and from 0.707 to 435 pg/mL for IL-6. Their specific roles in tumorigenesis are still unknown, but research has found that IL-6 expression affects DNA

methylation patterns, and its consistent expression results in the inactivation of tumor suppressor genes [26]. Furthermore, as a member of the cytokine family, IL-6 can recruit monocytes to the site of inflammation, triggering a chronic inflammatory response [26]. IL-8 persists longer at the inflammation site and improves tumor cell proliferation, facilitates tumor cell migration, and invasion [26]. Cancer cells also secrete IL-8 for the up-regulation of matrix metallopeptodase-7 that contributes to the epithelial-mesenchymal transition [23].

1.4 Optical biosensors as a potential tool for diagnostics

Despite the high resolution and accuracy of analytical methods for quantification of salivary proteins, they are constrained by high costs and the need for specialized laboratory settings, limiting their accessibility for widespread use. In contrast, optical sensors have emerged as an alternative due to their capacity for real-time analysis, high sensitivity, and potential for miniaturization. They also offer benefits such as low reagent usage, high signal clarity, and immunity to electromagnetic interference. What is more important, these advancements have paved the way for the parallel detection of multiple biomarkers in non-invasive biological fluids. Since more accurate assessment of disease state is provided by the behavior of a group of biomarkers, this will enhance the diagnostic efficiency of optical platforms.

In fact, not many studies have focused on parallel detection of OSCC biomarkers using optical sensors. For example, Kaminska *et al.* [33] in their research developed surface-enhanced Raman scattering (SERS)-based immunoassay that allowed them to detect IL-6, IL-8 and IL-18 levels in blood plasma samples. The integration of Au-Ag bimetallic nanoparticle surface enhanced sensitivity and sandwiched immunoassay with Raman reporter molecules improved the specificity to cytokines. Although this method is reliable and the multiplexing capabilities of the sensor are high, the complexity of sandwich immunoassay, similar to that of ELISA, and label-based detection mechanism can lead to challenges with precise washing steps, time-consuming detection with multiple incubation steps, and potential variability in signal intensity due to nanoparticle aggregation or nonuniform distribution of reporter molecules.

Another study by Dong *et al.* [34] developed an optical microfluidic biosensor with highly sensitive organic photodetectors that can detect eight proteins in parallel. Experiments with the device on cytokines such as IL-8, MMP-8 and IL-1β demonstrated LoD of 1.07 pM, 2.35 pM, and 4.57 pM respectively. Furthermore, they were able to perform detection on real

human saliva samples and compare the results with ELISA. The proposed sensor response correlated well with the ELISA results, offering advantages over bulky optical instrumentation.

There is a noticeable lack of research on sensors that demonstrate parallel detection of OSCC biomarkers in saliva samples. Most current approaches remain limited to single-analyte detection, which doesn't fully reflect the complex cancer environment. This highlights the significance of the present work where contribution to joint detection of salivary IL-6 and IL-8 is explored for the diagnosis of OSCC.

1.5 Framework of the study

This proof-of-concept study aims at developing an optical sensor based on semi-distributed interferometer (SDI) that will demonstrate high sensitivity and selectivity to salivary levels of IL-6 and IL-8. The current study doesn't involve real human saliva samples. Instead, the experiments are conducted using phosphate-buffered saline (PBS) doped with cytokines and subsequently in artificially saliva. This allows to assess the performance of the sensor in simplified and controlled way excluding all variables that may affect the response of the sensor. It is hypothesized that proposed sensing platform will demonstrate superior sensitivity, label-free detection capability, and real-time monitoring potential compared to conventional methods based on immunoassays, particularly for detecting low concentrations of biomarkers.

The objectives are:

- To fabricate and functionalize the semi-distributed interferometer-based optical biosensor;
- To assess the performance indicators of proposed biosensor using multi-resonance analysis in PBS doped with IL-6 and IL-8;
- To assess the performance of proposed biosensor using multi-resonance analysis in artificial saliva doped with IL-6 and IL-8;
- To assess specificity of the proposed biosensor using non-target proteins using cross-reactivity, TNF-α and CD44.

Chapter 2 – (Materials and Methods)

2.1 Materials

Phosphate Buffered Saline PBS (Sigma Aldrich, #P4417), sulfuric acid (SAFC, # 1.00713), hydrogen peroxide (Sigma Aldrich, #349887), methanol (Sigma Aldrich, #179337), (3-Aminopropyl)trimethoxysilane (APTMS) (Sigma Aldrich, #281778), glutaraldehyde (GA) (Sigma Aldrich, #340855), methoxypolyethylene glycol amine (m-PEG) (Sigma Aldrich, #07964).

Recombinant proteins and monoclonal antibodies were purchased from Cloud-Clone Corp. Monoclonal Antibody to Interleukin 8 (#MAA080Hu22), Monoclonal Antibody to Interleukin 6 (#MAA079Hu22), Recombinant Interleukin 8 (#RPA080Hu01), Recombinant Interleukin 6 (#RPA079Hu01)

2.2 Fabrication of semi-distributed interferometers (SDI)

The interferometers are fabricated in a similar way to the previous work [35]. The fabrication method implemented in the process can shortly be described as “splice-and-cleave”. The structure of the sensor is based on single-mode fiber (SMF-28) where the tip is the sensitive part to the surrounding’s refractive index. The sensitive part is provided by the enhanced backscattering fiber (EBF) which in our case is MgO nanoparticles doped fiber. In figure 2(a), two types of the fibers are aligned and spliced using standard telecom splicer (Fujikura 12-S). Then the sensing tip of around 1 mm is formed by manually cleaving EBF side of the spliced fibers with a single fiber cleaver (Fujikura CT-08). In order to differentiate between two types of fibers spliced together, the EBF side is colored using a dark colored marker. The result is the semi-distributed interferometer with the cavity having scattering centers that cause a set of distributed reflections.

2.3 Calibration of SDI

To assess the sensitivity of optical biosensor calibration is performed using sucrose solution. In total, 6 RI changes are detected by SDI including 1.3476, 1.3497, 1.3522, 1.3546, 1.3570 and 1.3585. 10 % sucrose solution corresponds to the lowest RI, and by adding increments of 400 µl of 40% sucrose solution five times other RI changes are obtained. The response of the sensor to RI is detected using Micron optics device where for wavelength range

of 1460 to 1620 nm the return loss (dBM) of each peak and valley is recorded. Experimental setup is shown in figure 2(b). The sensor is connected to the FBG analyzer (Micron Optics si255, VA, US) through FBG fiber to compensate for environmental fluctuations.

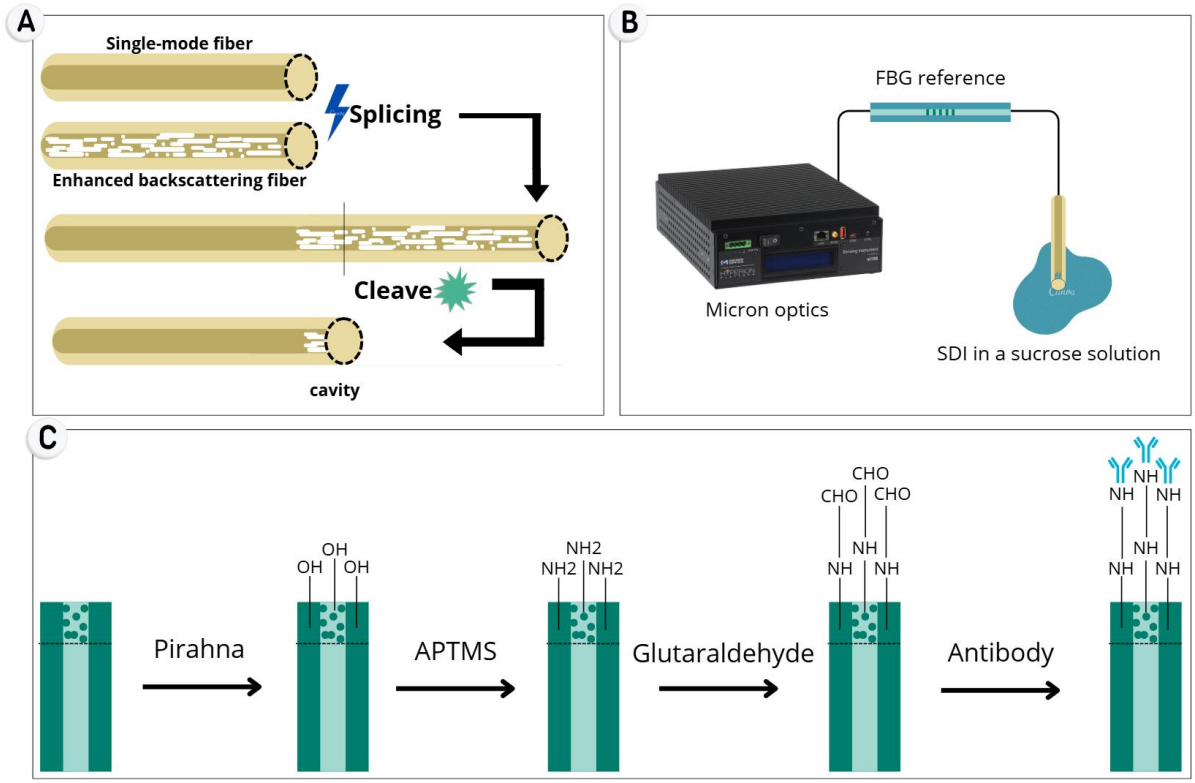

Figure 2. Artwork demostrating experimental setup and biofunctionalization. (a) The "splice-and-cleave" method of SDI sensor fabrication. (b) Sensor interrogation setup. (c) Biofunctionalization process detailing the modification steps.

2.4 Functionalization of SDI

The antibody attachment process begins by preparing the sensing tip through a series of treatments. Initially, the sensors are immersed in a Piranha solution (a mix of H_2SO_4 and H_2O_2 at a 4:1 ratio) for 15 minutes. Following thorough rinsing with water and air-drying, they are placed in a 1% APTMS solution in methanol for 20 minutes. The sensors are then heated in an oven at 110°C for one hour. After cooling, the sensors are incubated in a 25% GA solution in PBS for an additional hour. Antibodies are attached by immersing the sensors in a prepared antibody solution (4 µg/mL in PBS) for one hour. To prevent non-specific binding, the sensors are treated with a 10% m-PEG solution in PBS for 30 minutes. Finally, the prepared sensors are stored in PBS at 4°C until they are ready for use in detection. The schematic representation of this procedure is represented in figure 2(c). The surface analysis of functionalization used in

this work has been repeatedly described in previous works [36], [37], [38]. For this reason, in this work, it is not included.

2.5 Detection of IL-6 and IL-8 in media

Protein detection setup is similar to calibration step. The sensor is connected to Micron Optics device via FBG, and a tip is placed in a cap with media spiked with protein. Solutions of proteins with specific concentrations are prepared beforehand by serial dilution. For both proteins concentrations of 0 M, 10 aM, 1 fM, 100 fM, 10 pM, 1 nM, 100 nM are measured. The preparation of these solutions involve preparation of intermediate dilutions to minimize pipetting errors due to small sample solutions used in this biosensing assays. The information about the preparation of solutions is presented in Tables 1 and 2. The biosensor is incubated in each solution for 20 minutes and the data is saved each minute.

For specificity tests, the same setup and concentration range were implemented to ensure consistency. Functionalized sensors were used to measure the levels of TNF-α, CD44 and checked for cross-reactivity (IL-6 functionalized sensors were used in detection of IL-8 spiked solution and vice-versa). All the specificity tests were conducted using artificial saliva. The acquired data were analyzed using custom MATLAB scripts. The details of the analysis are covered in the next section.

Table 1. Serial dilution preparation planning for IL-6 spiked solution

Dilution	IL-6 volume, uL	Source	PBS or artificial saliva volume, uL	Concentration
1	1.88	from 21.28 uM working stock solution	398.12	100 nM
2	40	from dilution 1	360	10 nM
3	40	from dilution 2	360	1 nM
4	40	from dilution 3	360	100 pM
5	40	from dilution 4	360	10 pM
6	40	from dilution 5	360	1pM
7	40	from dilution 6	360	100 fM
8	40	from dilution 7	360	10 fM
9	40	from dilution 8	360	1 fM
10	40	from dilution 9	360	100 aM
11	40	from dilution 10	360	10 aM

Table 2. Serial dilution preparation planning for IL-8 spiked solution

Dilution	IL-8 volume, uL	Source	PBS or Artificial saliva volume, uL	Concentration
1	0.48	from 83.33 uM working stock solution	399.52	100 nM
2	40	from dilution 1	360	10 nM
3	40	from dilution 2	360	1 nM
4	40	from dilution 3	360	100 pM
5	40	from dilution 4	360	10 pM
6	40	from dilution 5	360	1pM
7	40	from dilution 6	360	100 fM
8	40	from dilution 7	360	10 fM
9	40	from dilution 8	360	1 fM
10	40	from dilution 9	360	100 aM
11	40	from dilution 10	360	10 aM

2.6 Data Analysis

SDI devices, as studied analytically [37] and experimentally [35] in previous work, are devices that produce a plurality of spectral features having random spectral spacing and intensity, each encoding the biological sensitivity. This approach results in rapid fabrication, but each sensor has a different spectral fingerprint. While in previous reports only the most significant spectral feature was extracted and analyzed, in this work we propose a multi-resonance analysis that exploits all the spectral features and their statistical distribution. This approach has three key advantages: (1) it removes the need for a manual analysis of a single feature, while this can be automated regardless of the spectral shape of each sensor; (2) it is more robust, since it accounts for all spectral features, and therefore it is more resilient to spectral distortions introduced by network elements (e.g. couplers, splitters, fiber attenuation); (3) in real case scenario, it makes the sensor less vulnerable to the power fluctuations.

The sketch of multi-resonance analysis is shown in Figure 3. The first step is to separate the spectral band of the FBG from the SDI fringes; the FBG is then used to compensate for temperature fluctuations and realign the spectrum. Within the SDI bands, all spectral features (peaks and valleys) are then estimated using $\geq$ 1.5 dB, which results in the SDI spectral envelope. The intensity change (ΔA) for each peak/valley is then studied, as the concentrations of IL-6/IL-8 increase, with respect to the reference condition. The intensity change for each spectral feature can then be analyzed, each having a different sensitivity. We perform a fit of

the whole spectral features dataset into a Gaussian probability density function (PDF) distribution: the mean value shows the intensity-changing trend of the whole set of features, while the standard deviation shows the sparsity of the concentration dependent sensitivity among the set of features. Then we can also perform a sensitivity analysis, reporting the statistical distribution of the IL-6/IL-8 sensitivity for each feature.

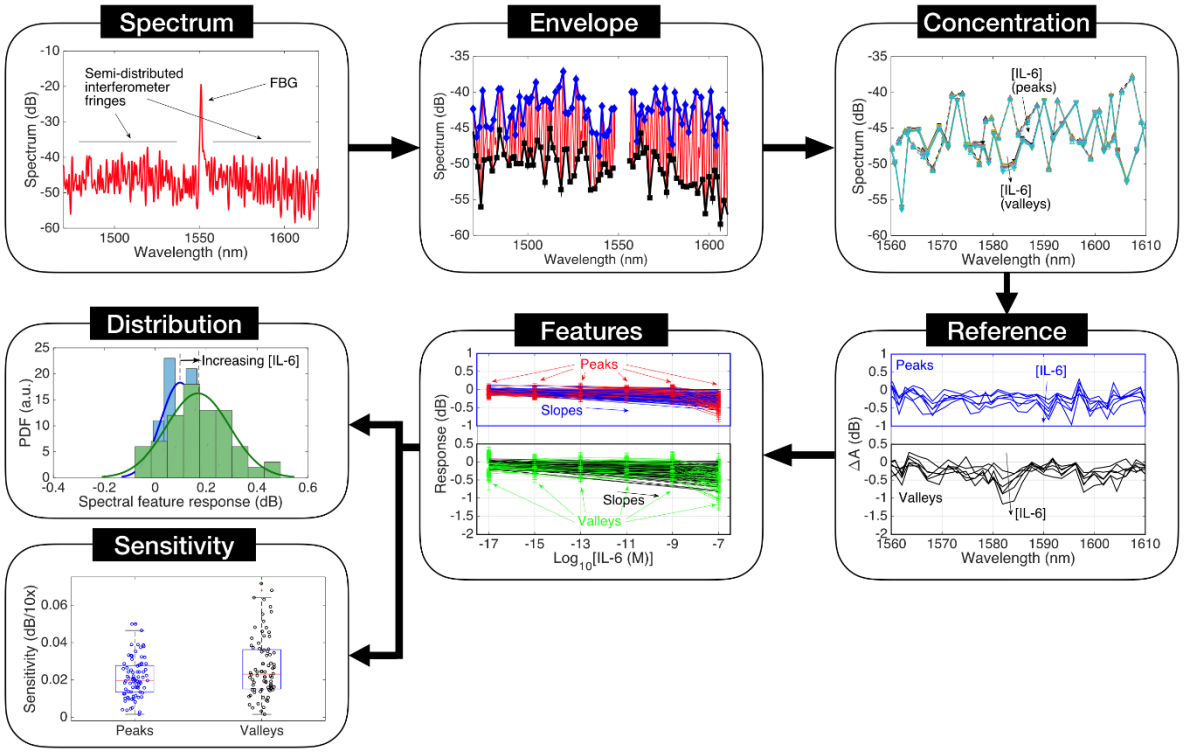

Figure 3. Visualization of the processing steps for multi-resonance analysis

2.7 Performance Indicators

Sensitivity estimation: log-linear regression for response in PBS; log-quadratic regression for response in saliva.

LoD estimation:

$$x_{LoD} = \Im^{-1}(y_{blank} + 3\sigma_{max}) \quad (1)$$

where xLoD = LoD concentration; $\Im$ = log-linear or log-quadratic input-output relation; yblank = blank level average response; σmax = maximum value of the one-sided standard deviation across all concentrations, for 20 consecutive measurements.

Repeatability: response measured for multiple SDI/FBG sensors, each fabricated from scratch on the same fiber and undergoing same functionalization. Responses are normalized (0%: lowest concentration; 100%: highest concentration) to account for different sensitivity.

Chapter 3 – (Results)

3.1 Detection of IL-6 in PBS

IL-6 doped in PBS detection was performed using an SDI-based sensor functionalized with anti-IL-6 antibodies with a maximum sensitivity of 163.86 dB/RIU that belongs to the valley between 1590 and 1600 nm of its spectrum. The sensor had around 80 valleys and peaks that were sensitive to small changes in RI, as proved after the calibration step. These random spectral features serve as a foundation for multi-resonance analysis, where intensity changes (ΔA) are extracted from relevant peaks and valleys to enhance detection sensitivity. The multi-resonance analysis was conducted on peaks and valleys separately, since the response to the change in concentration is different. The log-linear fit for valleys suggests that the intensity change is stable and consistent across all extracted valleys (Figure 4), whereas the log-quadratic fit for peaks reflects the nonuniform trend (Figure 5).

The spectrum of the sensor for IL-6 is presented in Figure 4(a) where the spectral variations at different concentrations are also added. The general trend is the downward shift of the spectrum as the concentration of the target protein increases. A closer look at the intensity changes for the extracted valleys is provided in Figure 4(b), which reflects the real-time dynamic intensity variations of each spectral valley. The figure shows a systematic shift in intensity towards the blue region, indicating an increase in RI as a result of a higher concentration and stronger protein binding. However, not all spectral features exhibit equal sensitivity to RI changes, which is confirmed in Figure 4(g), where individual valleys (green dots) show variability in their sensitivity. For this reason, some spectral features show less intense color changes over time (Figure 4(b)). Figure 4(c) summarizes the behavior of the spectral valleys by providing a visualization of PDF, reconstructed as a Gaussian distribution, where the color intensity represents the probability of a given ΔA at a specific time point. The density exhibits sharp transitions every 20 minutes, reflecting a change in protein concentration. Figure 4(d) reconstructs the PDF using IL-6 concentrations to show the trend in intensity change. Both figures agree that the distribution of intensity changes broadens over time, which corresponds to the increase in protein concentration and the resulting larger intensity variations across all spectral valleys. This suggests that certain spectral features are more responsive than others and reinforces the advantage of multi-resonance analysis over single-peak methods.

The overall trend of intensity change towards negative values is also evident from Figure 4(e), where the time-averaged response (blue line) shows a stepwise decrease in transmission intensity. This is also true for PDF visualizations depicted versus time (Figure 4(c)) and protein concentrations (Figure 4(d)), where intensity changes moved towards negative values. Due to environmental noise and variations in optical coupling, the real-time response (black line) exhibits fluctuations. The sensor exhibits excellent sensitivity and a strong correlation between IL-6 concentration and response, as confirmed by a LoD of 8.64 fM (Figure 4(f)).

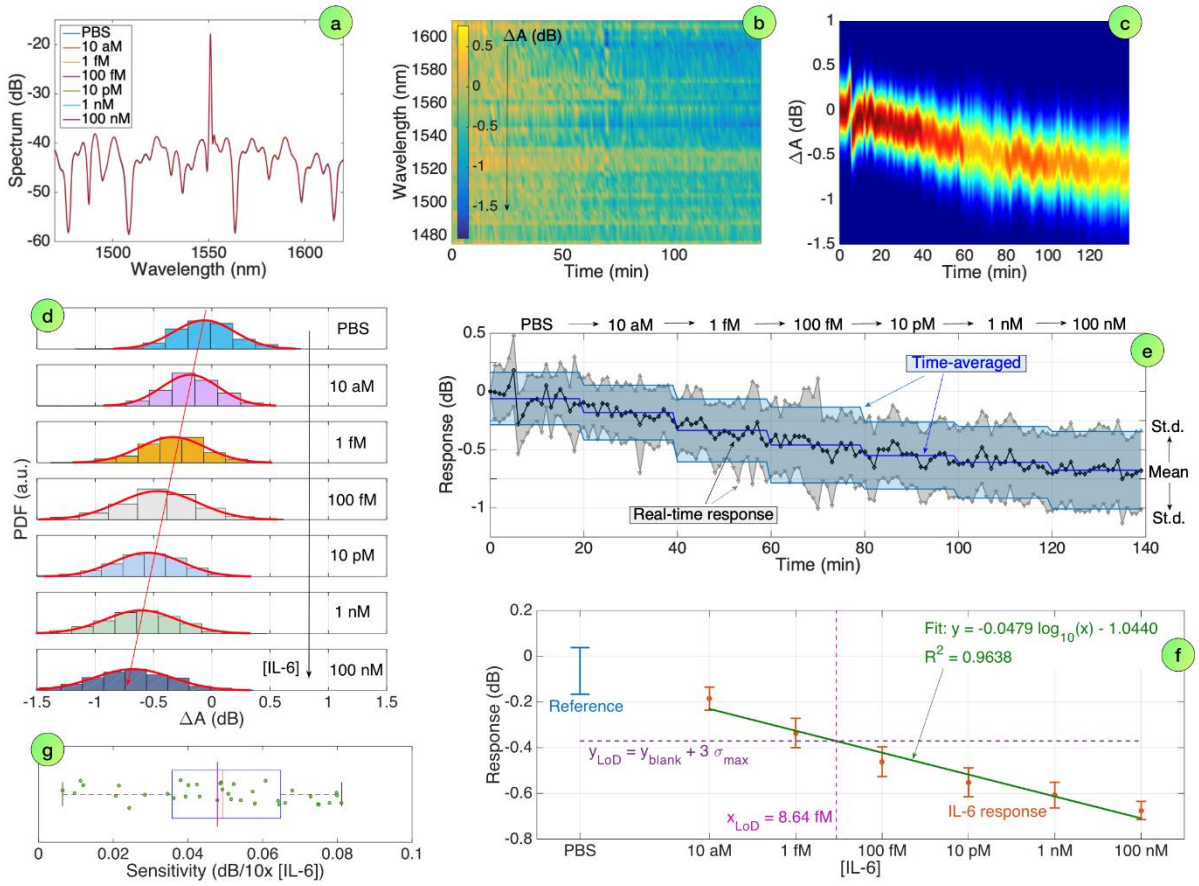

Figure 4. Detection of IL-6 protein in PBS, applying multi-resonance analysis to spectral valleys. (a) Spectrum of the SDI/FBG sensor for various concentrations of IL-6. (b) Variation of the intensity change for each identified spectral valley, varying the concentration each 20 minute. (c) Probability density function (PDF), reconstructed as a Gaussian function, across the experimental timeline. (d) PDF and its Gaussian distribution estimation for the intensity change of each spectral valley, for various IL-6 concentrations (10 aM to 100 nM). (e) Real-time dynamic response of the sensor to IL-6 concentration changes; shadow = two-sided standard deviation. (f) Response of the sensor to IL-6

concentration, estimating the sensitivity by log-linear regression and the detection limit; error bars = standard deviation of 20 consecutive measurements. (g) Estimated sensitivity for each spectral feature (boxplot and cloud), compared to the sensitivity obtained from multi-resonance analysis (purple line).

Despite the non-uniform trend of responses obtained by spectral peaks, the behavior of their PDF is similar – the intensity changes broaden over time as the concentration of protein increase (Figure 5(a)). The saturation of the response happens around 10 pM with a linear response at lower concentrations (Figure 5(d)). Therefore, the LoD calculated for spectral peaks (0.638 fM) is lower compared to the one obtained for spectral valleys.

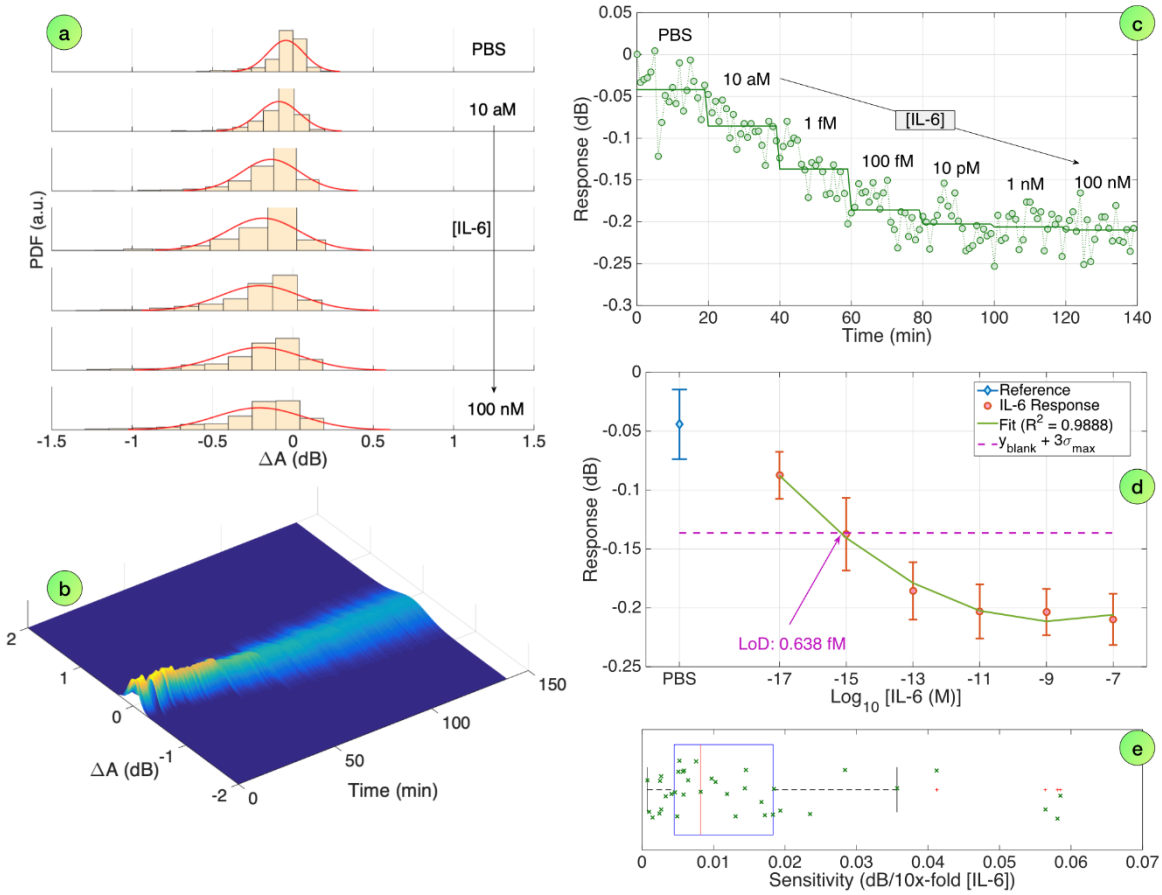

Figure 5. Visualization of the IL-6 detection in PBS, applying multi-resonance analysis to spectral peaks. (a) PDF and its Gaussian estimate for each IL-6 concentration. (b) Dynamic changes of the PDF over time. (c) Dynamic response of the sensor to various concentrations. (d) Response of the sensor to IL-6 concentration; sensitivity estimated using a log-quadratic fit. (e) Estimated sensitivity for each spectral feature.

Repeatability of the sensor was checked by observing response of the most significant spectral feature for nine sensors functionalized for the detection of IL-6. It was chosen to track the consistent and clear repeatability results which would be easier to interpret. Figure 6(a) shows the characteristic log-linear fit for the most significant feature, which is a valley or a peak that has the strongest correlation with the change in concetration of the protein. It can be seen that the response repeatability is high and varies between 10-20% (Figure 6(b)).

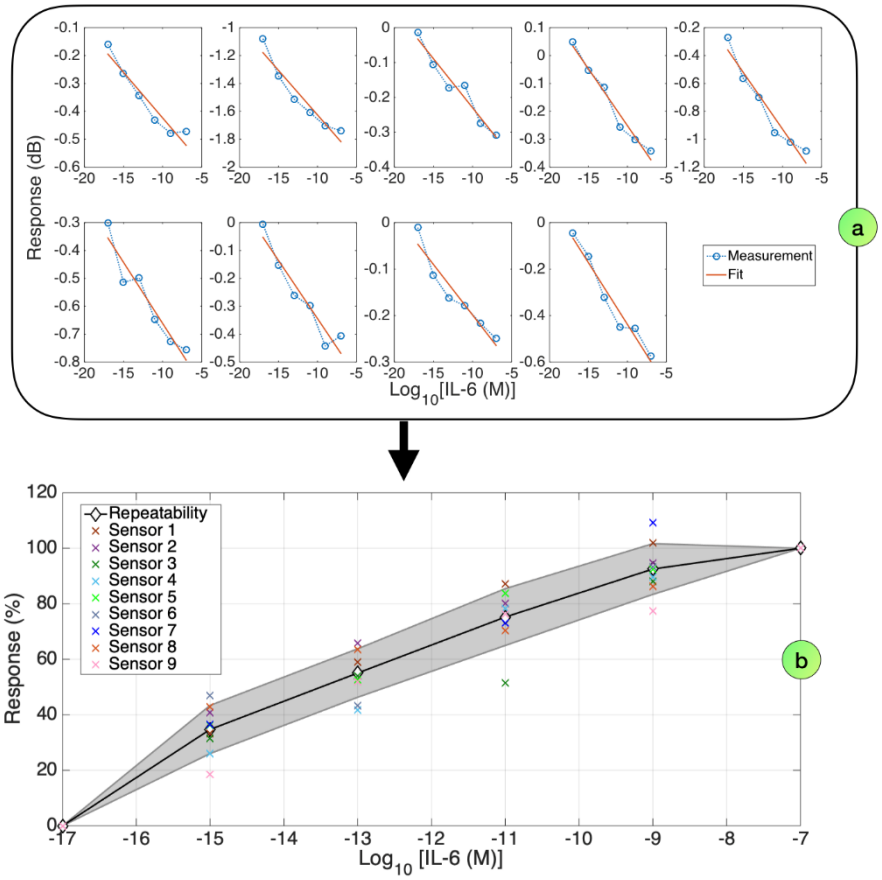

Figure 6. Repeatability observed for 9 sensors fabricated and biofunctionalized for IL-6 detection. (a) Response of the most significant spectral feature to concentration changes (10 aM to 100 nM), showing experimental data and log-linear fit. (b) Repeatability, obtained normalizing the responses of all sensors (range = standard deviation; solid line = average; 0% - lowest concentration; 100% = highest concentration).

3.2 Detection of IL-8 in PBS

The spectrum of SDI used for the detection of IL-8 is shown in Fig. 7(a). The maximum sensor sensitivity is 127.3171 dB/RIU. The distribution of spectral features is different from that of the previous sensor (Fig. 7(a)) which is expected due to random reflections in SDI.

However, the general trends observed for this sensor are similar to those previously observed with the IL-6 sensor. That is why only the main figures reflecting specific and fingerprint trends are shown in figure 7. Here, the PDF, reconstructed as the Gaussian distribution, is represented in a 3D figure showing the dependencies of ΔA for both time and IL-8 concentration simultaneously for precise visualization (Fig. 7(b)). The broadening of the PDF distribution is more evident in this sensor, with a systematic shift towards negative values, as expected. Compared to the previous sensor, this sensor has a higher proportion of spectral features that have lower sensitivities (Fig. 7(e)), which results in a greater broadening of the PDF as the overall response becomes more dispersed.

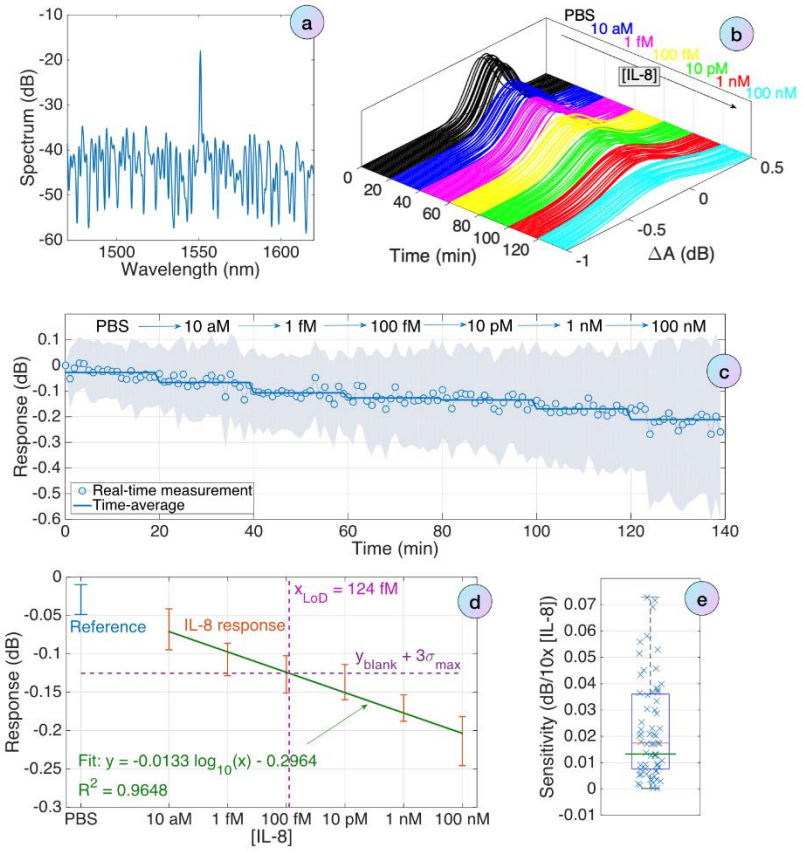

Figure 7. Detection of IL-8 protein in PBS. (a) Spectrum of the fabricated SDI/FBG biosensor. (b) Estimated PDF of the intensity change throughout the concentration increase from 10 aM to 100 nM. (c) Dynamic real-time response of the sensor, showing mean and two-sided standard deviation. (d) Response of the sensor to IL-8 concentrations, estimating sensitivity by log-linear regression. (e) Estimated sensitivity for each spectral feature (boxplot and cloud), compared to the sensitivity obtained from multi-resonance analysis (green line).

A similar trend as with the detection of IL-6 is observed from the real-time dynamic response (Fig. 7(c)). Although some deviations are present in the sensor response, the time-averaged response confirms the sensor's ability to track IL-8 concentration variations in real time. The LoD from the log-linear fit of the response is calculated to be 124 fM (Fig. 7(d)). The multi-resonance sensitivity of 0.0133 dB/10x [IL-8] from log-linear fit response (Fig. 7(d)) is lower than the sensitivity of certain individual spectral features or the median sensitivity obtained from the box plot (Fig. 7(e)). This is expected and true for all sensors in the analysis, since multi-resonance analysis includes the response for all spectral features regardless of their lower individual sensitivities. Incorporation of all spectral features reduces the susceptibility of single peak/valley with high sensitivity to noise, fabrication variability, and environmental fluctuations. This ensures a more robust and reproducible analysis of this detection method.

3.3 Detection of IL-6 and IL-8 in artificial saliva

Two channels of the interrogation device are used for the parallel detection of IL-6 and IL-8 in artificial saliva. The maximum sensitivities of SDI selected for functionalization are 117.87 dB/RIU and 124.83 dB/RIU for IL-6 and IL-8, respectively. The same steps of multi-resonance analysis were applied to construct figures (Fig. 8). To better visualize the comparison and account for parallel detection of analytes, the results for both sensors are shown in one figure. As expected, the behavior of the sensors in artificial saliva is similar to that observed in PBS. The PDF, reconstructed as a Gaussian function, shows a leftward shift and broadening of the distribution as concentration increases (Fig. 8(b)); the real-time response is stepwise (Fig. 8(c)). However, the intensity change for IL-8 is observed to be much larger from Fig. 8(c). There might be several reasons for this. First, from the estimated sensitivity for each spectral feature, the median sensitivity is larger for the IL-8 sensor (Fig. 8(h)). Furthermore, the molecular weight of the purchased recombinant human IL-8 is about four times lower, which may facilitate its receptor binding process and change in local RI.

The log-quadratic regression fit, with $R2 > 0.99$, obtained for both sensors is different from what was observed in PBS. This means that the response for each 10X increase in concentration is not uniform and, over time, the signal saturates leading to plateauing of intensity change. The corresponding LoD in artificial saliva is 480 aM and 23.4 fM for IL-6 and IL-8 respectively, as determined by log-quadratic regression fit (Fig. 8(f-g)). Fig. 8(d-e) accounts for the repeatability results in artificial saliva. The sensors have a high repeatability that varies from 18-40% for three IL-6 sensors and 17%-28% for three IL-8 sensors. A closer

look at the repeatability results can be observed in Figure 9. Three sensors for each type of protein were functionalized and used to identify most significant spectral features that will be used to estimate repeatability in artificial saliva.

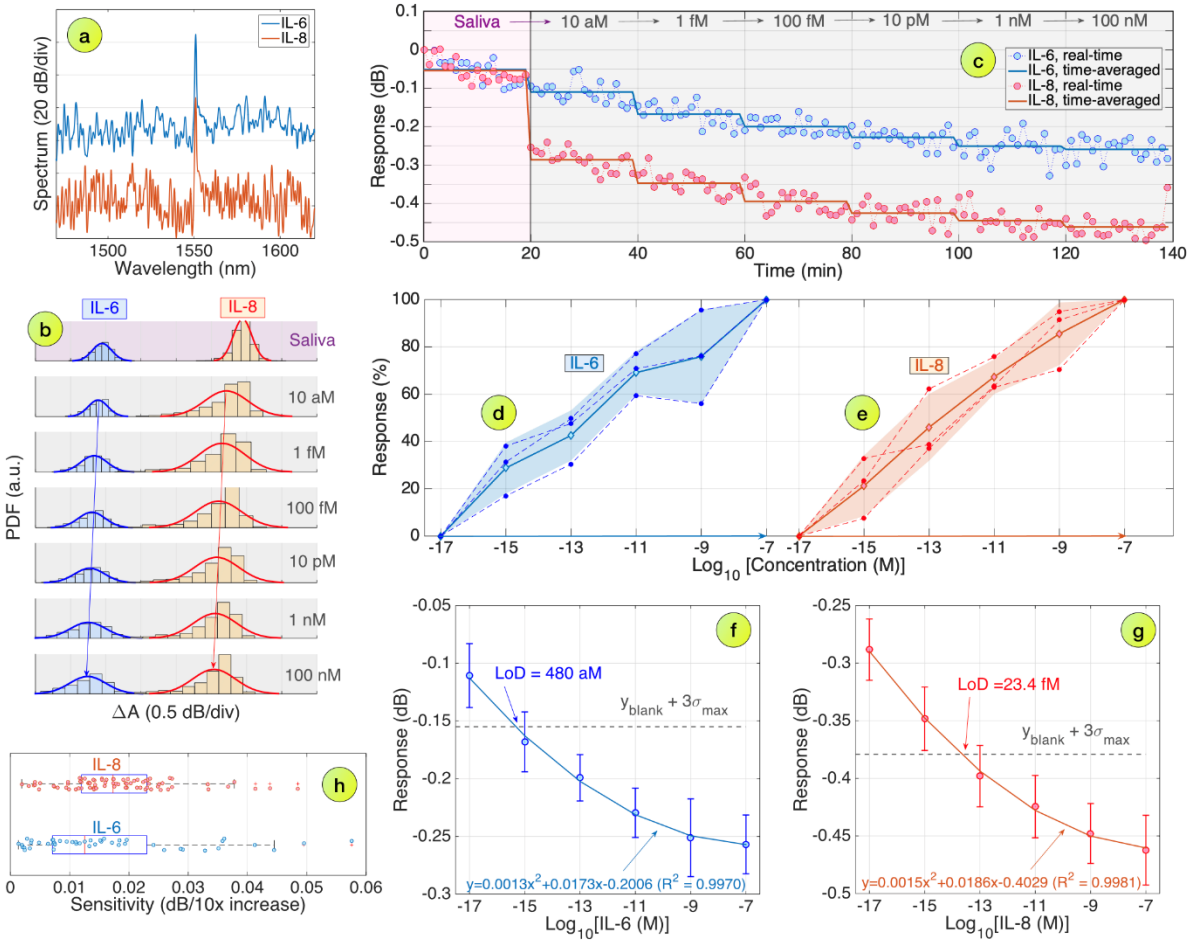

Figure 8. Detection of IL-6 and IL-8 proteins in artificial saliva. (a) Spectra of the biosensors fabricated for protein detection. (b) PDF and its Gaussian fit for the intensity detection estimated on all spectral features, for all protein concentrations. (c) Real-time responses of the sensors throughout the concentration changes (10 aM to 100 nM). (d-e) Repeatability of the sensors, observed by comparing the responses of 3 different sensors having same fabrication and functionalization. (f-g) Responses of the IL-6 and IL-8 sensors to protein concentration, using a log-quadratic fit and LoD estimation. (h) Estimated sensitivity for IL-6 and IL-8 sensors, evaluated for each spectral feature.

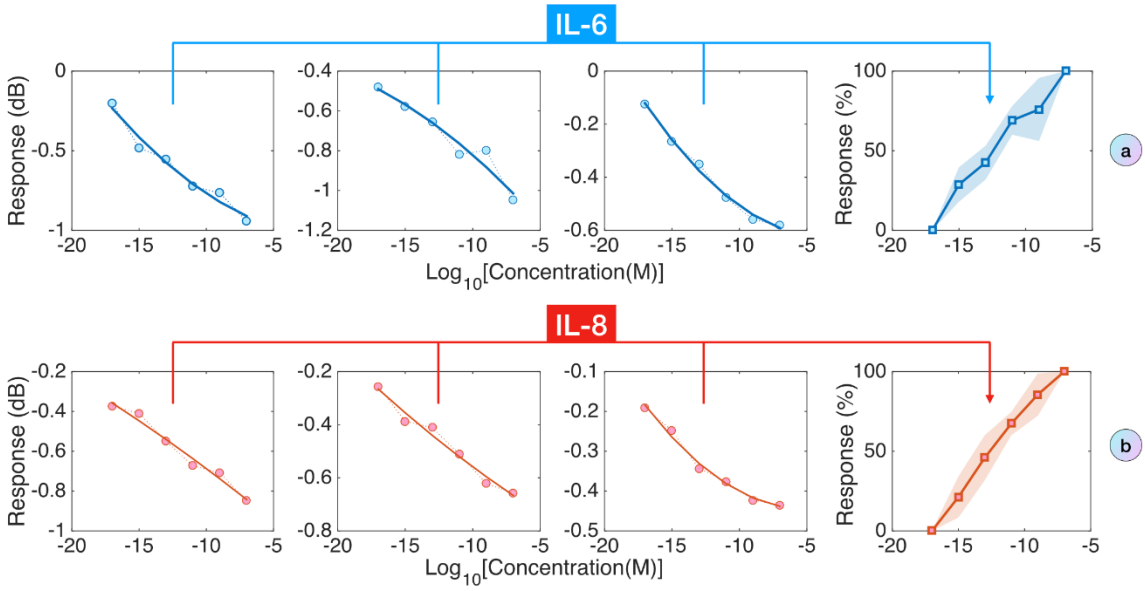

Figure 9. Repeatability observed for multiple sensors fabricated and biofunctionalized for IL-6 and IL-8 detection, measured in artificial saliva (3 sensors each). Repeatability is displayed normalizing the responses of the most significant spectral feature for all sensors (range = standard deviation; solid line = average; 0% - lowest concentration; 100% = highest concentration). (a) IL-6 repeatability; (b) IL-8 repeatability.

3.4 Specificity of IL-6 and IL-8 sensors

The specificity of the sensor was assessed by performing a detection procedure in artificial saliva doped with non-target proteins. The fabrication and functionalization procedures were the same for both the IL-6 and IL-8 sensors. Figure 10 compares the results of the detection in two forms. Figure 10(a) shows the overall log-linear response for the most significant spectral feature, and Figure 10(b) represents intensity changes obtained for specific concentrations for a more comprehensive overview of the results. Detection (in Figure10(a)) corresponds to the detection of the target protein in artificial saliva, cross-reactivity stands for the IL-6 and IL-8 protein detection procedure by a sensor functionalized oppositely, and the controls are CD44 and TNF-α proteins detection in artificial saliva. It is evident that negligible intensity changes are detected by the sensor with non-target protein detection for both control and cross-reactivity groups. Flatter regression slopes indicate negligible or no sensitivity to non-target proteins. This is further confirmed by looking at average intensity change values at given concentrations (Figure 10(b)). The strongest intensity changes are detected for the respective targets at all

concentrations. This effectively proves that the proposed sensors are highly selective and suitable for real-world applications.

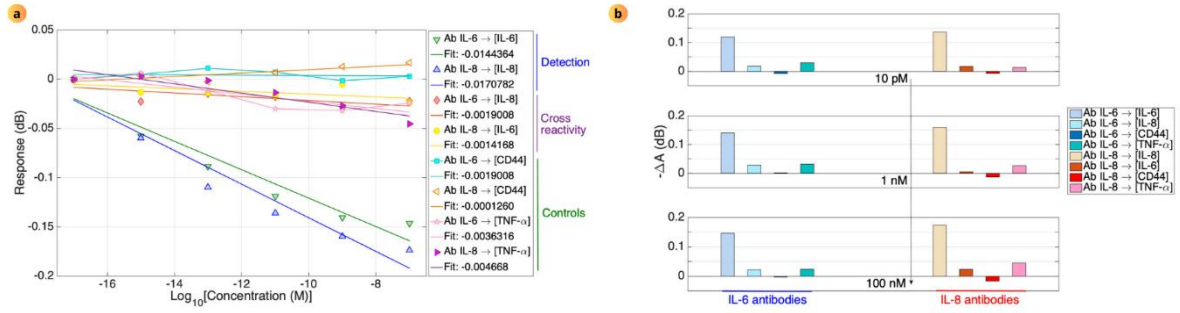

Figure 10. Specificity of SDI/FBG sensor. (a) Log-linear regression fit of the most significant spectral feature for IL-6 and IL-8 detection, cross-reactivity experiment and control (CD44 and TNF-α). (b) Intensity changes at 10 pM, 1 nM and 100 nM, comparing IL-6 and IL-8 sensor responses against target and non-target proteins

Chapter 4 – (Discussion)

Optical sensors have become a platform for detection of ultra-low concentrations of analytes and a promising tool in the development of point-of-care devices. Especially after the COVID-2019 pandemics, it has become evident that the rapid detection of biomarkers is critical for decentralized healthcare. This offers new possibilities for the accessibility of healthcare diagnostic systems in resource-limited or quarantine settings by providing quick, reliable, and actionable results. Saliva is particularly valuable diagnostic fluid in this sense, offering non-invasive, patient-friendly collection with minimal pre-treatment for diagnosis.

In this work, a multi-resonant analysis of protein detection was performed using an SDI-based optical sensor. The performance indicators obtained from this analysis supported the hypothesis stated in the introduction. As shown in Table 3, the proposed sensor demonstrates superior characteristics compared to most commercially available immunoassay kits.

Table 3. Performance indicators of commercially available ELISA kits.

Manufacturer, target	Minimal Reliable Detectable Concentration	Assay Range	Sample Volume	Catalog #
Invitrogen, Human IL-8	<5 pg/mL	15.6-1000 pg/mL	50 uL	KHC0081
Invitrogen, Human IL-8, uncoated ELISA kit	2 pg/mL	2-250 pg/mL	100 uL	88-8086
Invitrogen, Human IL-8 ProQuantum Immunoassay Kit	<0.01 pg/mL	0.0128 - 5000 pg/mL	2-5 uL	A35575

Millipore, Human IL-8	0.8 pg/mL	0.82-200 pg/mL	50 uL	EZHIL8
Aviva systems biology, Human IL-8	1.7 pg/mL	3.9-250pg/mL	50 uL	OKCD01311
Invitrogen, Human IL-6	<1 pg/mL	10.24-400 pg/mL	50 uL	EH2IL6
Invitrogen, Human IL-6 ProQuantum Immunoassay Kit	<0.05 pg/mL	0.064 - 10 ng/mL	2-5 uL	A35573
Millipore, Human IL-8	3 pg/mL	1.37-1000 pg/mL	50 uL	RAB0307
R&D Systems, Human IL-6	NA	9.4 - 600 pg/mL	100 uL	DY206
This work, IL-8	0.2808 pg/mL	0.12 pg/mL – 1.2 ug/mL	350 uL	NA
This work, IL-6	22.56 fg/mL	0.47 pg/mL - 4.7 ug/mL	350 uL	NA

NA – not applicable

The minimum reliably detectable concentration, or LoD, for the sensor developed in this work is lower than commercially available ELISA kits. They typically report a minimum reliably detectable concentration range of 1–5 pg/mL, as shown in Table 3. It is also important to highlight the differences in the curve-fitting approaches used to calculate this value. The sigmoidal model used for the optical sensor results reflects the typical behavior observed in biosensing, where signal saturation occurs due to limited binding site availability. In contrast, ELISA kits are optimized and manufactured to follow a linear model for ease of interpretation and use. As a result, they are often designed to operate within a limited concentration range.

This is reflected in Table 3 where the working concentration range is significantly broader for the proposed sensor than for ELISA kits.

The sigmoidal behavior of sensor response is consistent with a previously reported study of the detection of IL-8 in artificial saliva with a fiber-optic ball resonator [36]. They reported flattening of the signal near 10 fM, whereas in the presented work, flattening occurred at the highest detected concentration of 100 nM. One potential mechanism behind this saturation is the use of the same sensor for all serial dilutions; incomplete protein release from the antibody may prevent full regeneration between measurements. Another possible factor is the complex composition of artificial saliva where mucins and other biomolecules are present to mimic human saliva and its viscosity, potentially interfering with the target protein. However, the detected range is sufficient for measuring target protein levels in raw saliva without the need for dilution.

Our optical fiber-based biosensor offers a label-free detection approach, eliminating the need for enzyme-linked detection antibodies or fluorescence labeling. This simplifies the detection process and reduces the assay complexity. Compared to the sensors reported in Table 4, which represent recently developed biosensing platforms for the parallel detection of several cytokines, our biosensor demonstrates superior performance in terms of LoD, reaching the femtogram level and offering high sensitivity for detecting low-concentration biomarkers. The proposed method also offers advantages over biosensors based on electrochemical impedance spectroscopy (EIS). Optical sensors provide higher sensitivity, allowing for detection of ultra-low analyte concentrations. Furthermore, optical sensors are resistant to electromagnetic interference, unlike EIS-based sensors. These advantages of the proposed optical biosensor position it as a promising platform for rapid and highly sensitive biomarker detection in complex biofluids.

However, the observed sensitivities for the developed sensor are much lower than previously reported weak reflector tip fiber-optic ball resonator sensors using a similar functionalization method [36]. They reported a sensitivity of 0.091 dB per 10-fold increase in target protein concentration, with a LoD of 4.68 aM. However, SDI sensors offer advantages in terms of easier and faster fabrication as well as cost-effective, telecom-fiber oriented detection. In this work, detection is performed using a commercially available FBG interrogator, allowing for a scalable and more accessible approach.

Table 4. Different biosensors for the detection of interleukins from literature

Detection method	Targets	Limit of detection	Studied concentration range	Media	Ref.
SERS-based multiplexed immunoassay	IL-6, IL-8 and IL-18	IL-6: 2.3 pg/mL IL-8: 6.5 pg/mL IL-18: 4.2 pg/mL	0-30 ng/mL	Plasma	[33]
Photodetector-based optical microfluidic biosensor	IL-8, IL-1β, and MMP-8	between 80 pg/mL and 120 pg/mL	NA	Artificial saliva	[34]
SERS-based dot-blot immunoassay	IL-6 and IL-8	1 pg/mL (IL-6)	1 pg/mL-10 ng/mL	NA	[39]
Fiber-optic microsphere-based antibody array	IL-6 and IL-8	1.344 pg/mL and 64 fg/mL	30 pg/mL to 10.5 μg/mL	PBS	[40]
EIS-based on nanotube titanium dioxide array	IL-6, IL-8 and TNF-α	5 pg/mL each	0-2500 pg/mL	PBS	[41]
Lateral flow-based EIS	IL-6 and IL-8	1 pg/mL each	IL-6: 1-100 pg/mL IL-8: 1-1000 pg/mL	Urine	[42]
Optical fiber-based fluorescent biosensor	IL-6	1 pg/mL	0-200 pg/mL	Serum	[43]
Confocal optics-based micro-sensor	IL-8	4 fM	6 fM – 12 pM	PBS	[44]
SDI sensor	IL-6 and IL-8	IL-6: 480 aM (22.56 fg/mL) IL-8: 23.4 fM (0.2808 pg/mL)	10 aM – 100 nM	Artificial saliva	This work

Chapter 5 – (Conclusion)

In this work, the multi-resonance analysis of an FBG-assisted SDI-based probe-shaped sensor is presented. The sensor demonstrated selective detection of OSCC biomarkers in artificial saliva, achieving a LoD of 480 aM for IL-6 and 23.4 fM for IL-8. It successfully confirmed the ability to distinguish non-target proteins (CD44 and TNF-α). The comparison of the performance indicators with commercially available ELISA kits showed that the developed sensor offers better LoD and working range. Additionally, the multi-resonance approach that leverages the entire spectral response rather than a single spectral feature enhances the robustness and resilience to spectral distortions. The future work should focus on validating the sensor's performance in clinical saliva samples and demonstrating that under real-world implications the multi-resonance analysis makes the sensor less vulnerable to the power fluctuations.

Reference List

[1] M. A. Javaid, A. S. Ahmed, R. Durand, and S. D. Tran, “Saliva as a diagnostic tool for oral and systemic diseases,” *J Oral Biol Craniofac Res*, vol. 6, no. 1, p. 66, Jan. 2015, doi: 10.1016/J.JOBCR.2015.08.006.

[2] Z. Huang *et al.*, “Saliva - A new opportunity for fluid biopsy,” Jan. 01, 2023, *De Gruyter Open Ltd*. doi: 10.1515/cclm-2022-0793.

[3] P. Gopikrishna, A. Ramesh kumar, K. Rajkumar, R. Ashwini, and S. Venkatkumar, “Saliva: A potential diagnostic tool for oral cancer and oral diseases - A detailed review,” *Oral Oncology Reports*, vol. 10, p. 100508, Jun. 2024, doi: 10.1016/J.OOR.2024.100508.

[4] S. Kumari *et al.*, “A Review on Saliva-Based Health Diagnostics: Biomarker Selection and Future Directions,” Mar. 01, 2024, *Springer Nature*. doi: 10.1007/s44174-023-00090-z.

[5] E. Macchia *et al.*, “Selective single-molecule analytical detection of C-reactive protein in saliva with an organic transistor,” *Anal Bioanal Chem*, vol. 411, no. 19, pp. 4899–4908, Jul. 2019, doi: 10.1007/S00216-019-01778-2/FIGURES/3.

[6] Y. Cui *et al.*, “Developments in diagnostic applications of saliva in human organ diseases,” *Med Nov Technol Devices*, vol. 13, p. 100115, Mar. 2022, doi: 10.1016/J.MEDNTD.2022.100115.

[7] S. P. Humphrey and R. T. Williamson, “A review of saliva: Normal composition, flow, and function,” *Journal of Prosthetic Dentistry*, vol. 85, no. 2, pp. 162–169, Feb. 2001, doi: 10.1067/MPR.2001.113778.

[8] H. Mortazavi, A. A. Yousefi-Koma, and H. Yousefi-Koma, “Extensive comparison of salivary collection, transportation, preparation, and storage methods: a systematic review,” *BMC Oral Health*, vol. 24, no. 1, pp. 1–30, Dec. 2024, doi: 10.1186/S12903-024-03902-W/FIGURES/2.

[9] J. M. H. Fey, F. J. Bikker, and D. Hesse, “Saliva Collection Methods Among Children and Adolescents: A Scoping Review,” *Mol Diagn Ther*, vol. 28, no. 1, pp. 15–26, Jan. 2024, doi: 10.1007/S40291-023-00684-9/FIGURES/2.

[10] F. G. Bellagambi *et al.*, “Saliva sampling: Methods and devices. An overview,” *TrAC Trends in Analytical Chemistry*, vol. 124, p. 115781, Mar. 2020, doi: 10.1016/J.TRAC.2019.115781.

[11] I. T. Gug, M. Tertis, O. Hosu, and C. Cristea, “Salivary biomarkers detection: Analytical and immunological methods overview,” *TrAC Trends in Analytical Chemistry*, vol. 113, pp. 301–316, Apr. 2019, doi: 10.1016/J.TRAC.2019.02.020.

[12] Y.-C. Hsiao *et al.*, “Variability Assessment of 90 Salivary Proteins in Intraday and Interday Samples from Healthy Donors by Multiple Reaction Monitoring-Mass Spectrometry,” *Proteomics Clin Appl*, vol. 12, no. 2, p. 1700039, Mar. 2018, doi: 10.1002/PRCA.201700039.

[13] P. Grocholska, M. Kowalska, and R. Bąchor, “Qualitative and Quantitative Mass Spectrometry in Salivary Metabolomics and Proteomics,” Feb. 01, 2023, *MDPI*. doi: 10.3390/metabo13020155.

[14] T. Dong *et al.*, “Advances in Electrochemical Biosensors Based on Nanomaterials for Protein Biomarker Detection in Saliva,” *Advanced Science*, vol. 10, no. 6, p. 2205429, Feb. 2023, doi: 10.1002/ADVS.202205429.

[15] R. Antonelli *et al.*, “Salivary metabolomics in oral cancer: A systematic review,” *Oral Oncology Reports*, vol. 11, p. 100657, Sep. 2024, doi: 10.1016/J.OOR.2024.100657.

[16] H. Sung *et al.*, “Global Cancer Statistics 2020: GLOBOCAN Estimates of

Incidence and Mortality Worldwide for 36 Cancers in 185 Countries," *CA Cancer J Clin*, vol. 71, no. 3, pp. 209–249, May 2021, doi: 10.3322/CAAC.21660.

[17] Y. Tan *et al.*, "Oral squamous cell carcinomas: state of the field and emerging directions," *International Journal of Oral Science 2023 15:1*, vol. 15, no. 1, pp. 1–23, Sep. 2023, doi: 10.1038/s41368-023-00249-w.

[18] T. Dineshkumar, B. K. Ashwini, A. Rameshkumar, P. Rajashree, R. Ramya, and K. Rajkumar, "Salivary and serum interleukin-6 levels in oral premalignant disorders and squamous cell Carcinoma: Diagnostic value and clinicopathologic correlations," *Asian Pacific Journal of Cancer Prevention*, vol. 17, no. 11, pp. 4899–4906, Nov. 2016, doi: 10.22034/APJCP.2016.17.11.4899.

[19] S. Ramachandran, "Oral cancer: Recent breakthroughs in pathology and therapeutic approaches," *Oral Oncology Reports*, vol. 12, p. 100678, Dec. 2024, doi: 10.1016/J.OOR.2024.100678.

[20] T. Guenzel, A. Franzen, … S. W.-A., and undefined 2013, "The value of PET compared to MRI in malignant head and neck tumors," *ar.iiarjournals.orgT Guenzel, A Franzen, S Wiegand, S Kraetschmer, JL Jahn, R Mironczuk, T WilhelmAnticancer research, 2013•ar.iiarjournals.org*, Accessed: Nov. 23, 2024. [Online]. Available: https://ar.iiarjournals.org/content/33/3/1141.short

[21] S. Aulakh, D. Silverman, K. Young, S. D.- Cancers, and undefined 2022, "The promise of circulating tumor DNA in head and neck cancer," *mdpi.comSS Aulakh, DA Silverman, K Young, SK Dennis, AC BirkelandCancers, 2022•mdpi.com*, Accessed: Nov. 23, 2024. [Online]. Available: https://www.mdpi.com/2072-6694/14/12/2968

[22] V. Dikova, E. Jantus-Lewintre, and J. Bagan, "Potential Non-Invasive Biomarkers for Early Diagnosis of Oral Squamous Cell Carcinoma," *J Clin Med*, vol. 10, no. 8, p. 1658, Apr. 2021, doi: 10.3390/JCM10081658.

[23] K. Smriti *et al.*, "Salivary MMP-9 as a biomarker for the diagnosis of oral potentially malignant disorders and oral squamous cell carcinoma," *Asian Pacific Journal of Cancer Prevention*, vol. 21, no. 1, pp. 233–238, Jan. 2020, doi: 10.31557/APJCP.2020.21.1.233.

[24] N. Mehterov *et al.*, "Salivary miR-30c-5p as potential biomarker for detection of oral squamous cell carcinoma," *mdpi.comN Mehterov, B Vladimirov, A Sacconi, C Pulito, M Rucinski, G Blandino, V SarafianBiomedicines, 2021•mdpi.com*, vol. 9, no. 9, 2021, doi: 10.3390/biomedicines9091079.

[25] A. Roi, C. I. Roi, M. L. Negruțiu, M. Riviș, C. Sinescu, and L. C. Rusu, "The Challenges of OSCC Diagnosis: Salivary Cytokines as Potential Biomarkers," *J Clin Med*, vol. 9, no. 9, p. 2866, Sep. 2020, doi: 10.3390/JCM9092866.

[26] S. Ekmekcioglu, R. Kurzrock, and E. A. Grimm, "Hematopoietic Growth Factors and Cytokines," *The Molecular Basis of Cancer: Fourth Edition*, pp. 789-808.e4, 2014, doi: 10.1016/B978-1-4557-4066-6.00057-3.

[27] I. Alevizos *et al.*, "Oral cancer in vivo gene expression profiling assisted by laser capture microdissection and microarray analysis," *Oncogene*, vol. 20, no. 43, pp. 6196–6204, Sep. 2001, doi: 10.1038/sj.onc.1204685.

[28] M. A. R. St. John *et al.*, "Interleukin 6 and Interleukin 8 as Potential Biomarkers for Oral Cavity and Oropharyngeal Squamous Cell Carcinoma," *Arch Otolaryngol Head Neck Surg*, vol. 130, no. 8, pp. 929–935, Aug. 2004, doi: 10.1001/ARCHOTOL.130.8.929.

[29] P. C. Heinrich, I. Behrmann, G. Müller-Newen, F. Schaper, and L. Graeve, "Interleukin-6-type cytokine signalling through the gp130/Jak/STAT pathway.," *Biochemical Journal*, vol. 334, no. Pt 2, p. 297, Sep. 1998, doi:

10.1042/BJ3340297.

[30] S. Ekmekcioglu, R. Kurzrock, and E. A. Grimm, “Hematopoietic Growth Factors and Cytokines,” *The Molecular Basis of Cancer*, pp. 605–619, Jan. 2008, doi: 10.1016/B978-141603703-3.10051-2.

[31] “IL-8, a novel messenger to cross-link inflammation and tumor EMT via autocrine and paracrine pathways (Review).” Accessed: Sep. 15, 2024. [Online]. Available: https://www.spandidos-publications.com/10.3892/ijo.2015.3234#b18-ijo-48-01-0005

[32] M. M. A. Chiamulera, C. B. Zancan, A. P. Remor, M. F. Cordeiro, F. O. Gleber-Netto, and A. R. Baptistella, “Salivary cytokines as biomarkers of oral cancer: a systematic review and meta-analysis,” *BMC Cancer*, vol. 21, no. 1, pp. 1–16, Dec. 2021, doi: 10.1186/S12885-021-07932-3/FIGURES/4.

[33] A. Kamińska *et al.*, “SERS-based Immunoassay in a Microfluidic System for the Multiplexed Recognition of Interleukins from Blood Plasma: Towards Picogram Detection,” *Scientific Reports 2017 7:1*, vol. 7, no. 1, pp. 1–11, Sep. 2017, doi: 10.1038/s41598-017-11152-w.

[34] T. Dong and N. M. M. Pires, “Immunodetection of salivary biomarkers by an optical microfluidic biosensor with polyethylenimine-modified polythiophene-C70 organic photodetectors,” *Biosens Bioelectron*, vol. 94, pp. 321–327, Aug. 2017, doi: 10.1016/J.BIOS.2017.03.005.

[35] S. Kazhiyev, A. Abdossova, D. Moldabay, A. Rakhimbekova, W. Blanc, and D. Tosi, “Semi-distributed interferometers fiber-optic sensors for high-sensitivity refractive index detection: Design and sensitivity analysis,” *Measurement*, vol. 220, p. 113327, Oct. 2023, doi: 10.1016/J.MEASUREMENT.2023.113327.

[36] G. Rashidova, M. Tilegen, T. T. Pham, A. Bekmurzayeva, D. Tosi, and D. Tosi, “Functionalized optical fiber ball-shaped biosensor for label-free, low-limit detection of IL-8 protein,” *Biomedical Optics Express, Vol. 15, Issue 1, pp. 185-198*, vol. 15, no. 1, pp. 185–198, Jan. 2024, doi: 10.1364/BOE.504780.

[37] A. Rakhimbekova *et al.*, “Fiber-optic semi-distributed Fabry-Perot interferometer for low-limit label-free detection of CCL5 cancer biomarker,” *Opt Laser Technol*, vol. 168, p. 109953, Jan. 2024, doi: 10.1016/J.OPTLASTEC.2023.109953.

[38] A. Abdossova *et al.*, “Detection of vaccinia virus proteins in wastewater environment using biofunctionalized optical fiber semi-distributed FBG-assisted interferometric probes,” *Sens Biosensing Res*, vol. 46, p. 100699, Dec. 2024, doi: 10.1016/J.SBSR.2024.100699.

[39] Y. Wang, M. Salehi, M. Schütz, and S. Schlücker, “Femtogram detection of cytokines in a direct dot-blot assay using SERS microspectroscopy and hydrophilically stabilized Au–Ag nanoshells,” *Chemical Communications*, vol. 50, no. 21, pp. 2711–2714, Feb. 2014, doi: 10.1039/C3CC48633H.

[40] T. M. Blicharz *et al.*, “Fiber-optic microsphere-based antibody array for the analysis of inflammatory cytokines in saliva,” *Anal Chem*, vol. 81, no. 6, pp. 2106–2114, Mar. 2009, doi: 10.1021/AC802181J/SUPPL_FILE/AC802181J_SI_001.PDF.

[41] K. Arkusz and E. Paradowska, “Impedimetric Detection of Femtomolar Levels of Interleukin 6, Interleukin 8, and Tumor Necrosis Factor Alpha Based on Thermally Modified Nanotubular Titanium Dioxide Arrays,” *Nanomaterials 2020, Vol. 10, Page 2399*, vol. 10, no. 12, p. 2399, Nov. 2020, doi: 10.3390/NANO10122399.

[42] A. Ganguly, V. Gunda, K. Thai, and S. Prasad, “Inflammatory Stimuli Responsive Non-Faradaic, Ultrasensitive Combinatorial Electrochemical Urine

Biosensor," *Sensors (Basel)*, vol. 22, no. 20, Oct. 2022, doi: 10.3390/S22207757.

[43] G. Liu, K. Zhang, A. Nadort, M. R. Hutchinson, and E. M. Goldys, "Sensitive Cytokine Assay Based on Optical Fiber Allowing Localized and Spatially Resolved Detection of Interleukin-6," vol. 2, pp. 218–226, 2017, doi: 10.1021/acssensors.6b00619.

[44] W. Tan *et al.*, "Optical Protein Sensor for Detecting Cancer Markers in Saliva," *Biosens Bioelectron*, vol. 24, no. 2, p. 266, Oct. 2008, doi: 10.1016/J.BIOS.2008.03.037.